Inherent limit to coherent phonon generation under nonresonant light-field driving

K. Uchida [*], K. Nagai, N. Yoshikawa, and K. Tanaka[†]

Department of Physics, Graduate School of Science, Kyoto University, Kyoto, Kyoto 606–8502, Japan

Coherent manipulation of quasiparticles is a crucial method to realize ultrafast switching of the relating macroscopic order. In this paper, we studied coherent phonon generation under strong light field which allows one to induce nonperturbative nonlinear optical phenomena in solids. The efficiency of coherent phonon generation starts to saturate and deviate from the pronounced linear power dependence when the light intensity goes into the nonperturbative regime. It is clarified that the deviation is not originated from the absorption saturation due to the real incoherent carrier generation. We propose a theoretical model based on the Floquet picture and show that the saturation is due to a limitation of the driving force inherent in nonresonant driving of the electronic system in the nonperturbative regime.

Intense laser-field driving of solid materials may give rise to a novel nonequilibrium state that has the potential to show new functionality and induce phase-transition phenomena [1,2]. This can be realized through a large-amplitude excitation of a phonon system, and this capability has given rise to the study of nonlinear phononics [3,4]. One promising driving method for the phonon mode is the impulsive stimulated Raman scattering (ISRS) process [5,6], where ultrashort-pulse excitation in a nonresonant relation to the electronic transition generates an impulsive force through electron-phonon coupling. In the perturbation limit, ISRS gives a driving force proportional to the light intensity [5,6]. It is a crucial problem for the realization of nonlinear phononics how a large-amplitude phonon mode can be realized through electron-phonon coupling using extremely strong light beyond the range in which perturbation theory applies (nonperturbative nonlinear regime) [7].

The recent development of femtosecond laser technology in the midinfrared (MIR) region enables us to step into a nonperturbative nonlinear regime in solids without damaging and heating the sample. In this regime, the electronic energy is significantly modified, and highly nonlinear optical responses such as high-order harmonic generation (HHG) appear [8–12]. Thus, this technology has made it possible to conduct experiments aimed at answering the question of whether there is a limit to the driving force of coherent phonon generation under nonresonant conditions.

Here, we study coherent phonon generation induced by using intense MIR laser field ($\hbar\Omega_{\mathrm{MIR}} = 0.26$ eV), which drives an electronic system strongly without creating incoherent carriers nor damaging the sample. The maximum intensity at the sample position was 0.6 TW/cm^2 in air, corresponding to an electric field of $E_{\mathrm{MIR}} = 13$ MV/cm inside the sample. The sample was a single crystal of 100-μm-thick gallium selenide

(GaSe), which shows efficient HHG emission, i.e., strong light-electron interactions [13–15]. Since the photon energy of the MIR pulse (0.26 eV) is much larger than the phonon energy in GaSe (<0.04 eV) [16], direct excitation of phonon modes is sufficiently suppressed. Figure 1(a) shows the experimental setup of the HHG measurement in transmission geometry. We performed experiments with MIR polarizations parallel and perpendicular to the vertical mirror plane of the crystal (A-pol and Z-pol, respectively). The measured HHG spectra are shown in Fig. 1(b). We observed HHG from 5th to 12th orders and found that HHG with A-pol is stronger than that with Z-pol, which is consistent with previous research [15]. Figure 1(c) shows the MIR intensity dependence of fifth-order harmonic intensity. Above 0.3 TW/cm^2, the plot starts to deviate from a power law ($I_{\mathrm{HHG}} \propto I_{\mathrm{MIR}}^5$), indicating that the light-electron interaction enters the nonperturbative nonlinear regime.

Under such an extremely nonlinear condition, we performed MIR-pump and near-infrared (NIR)-probe ($\hbar\Omega_{\mathrm{NIR}} = 1.55$ eV) measurements, as depicted in Fig. 2(a), to observe coherent phonons in GaSe [6,17]. Note that the nonlinear propagation effect of MIR pump, which veils the intrinsic coherent phonon signal, is negligible in our experimental conditions [18]. The transmitted NIR probe pulses were detected in a polarization-resolved manner, which is a similar technique to the electro-optic sampling method [20]. Figure 2(b) plots the pump-probe signal as a function of the time delay T between MIR pump and NIR probe pulses. After the impulsive response at $T = 0$ ps, which may be attributed to a third order or higher nonlinear coherent optical process, two kinds of oscillations with different frequencies appear clearly. The faster oscillation decays within 10 ps, while the slower one continues to oscillate for least 100 ps. Figure 2(c) shows the Fourier-transformed spectrum of the signal, in which there are two distinct peaks at frequencies of 0.6 and 4.0 THz corresponding to the temporal oscillations. These frequencies are, respectively, attributed to the E' shearing mode and A'_1 breathing mode depicted in Fig. 2(d) [21]. The background

* Corresponding author: uchida.kento.4z@kyoto-u.ac.jp
† Corresponding author: kochan@scphys.kyoto-u.ac.jp
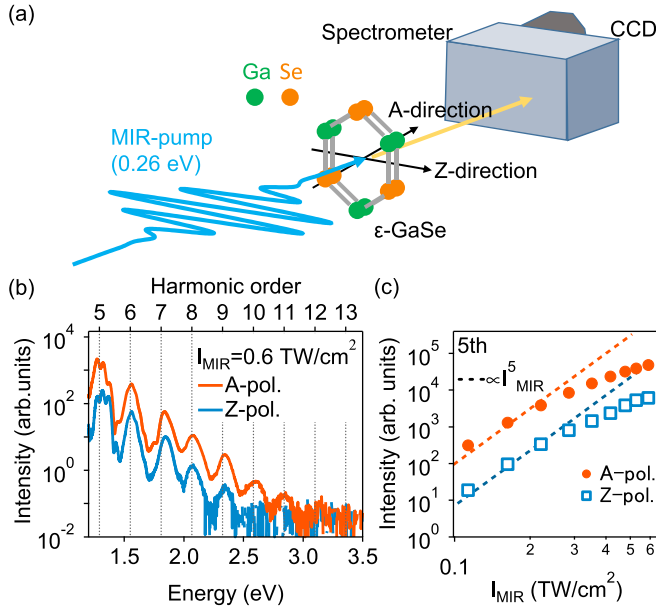
FIG. 1. HHG in GaSe crystal. (a) Setup of HHG experiment in transmission geometry. The MIR polarization parallel (perpendicular) to the mirror plane of the crystal is denoted as the A-(Z-) polarization. (b) HHG spectra in visible region with A-pol (orange solid line) and Z-pol (blue solid line). (c) MIR intensity dependence of fifth-order HHG intensity with A-pol (orange circles) and Z-pol (blue open squares). Dashed lines are guides for the eye that are proportional to the fifth power of MIR intensity.

signal due to incoherent carrier generation is negligible compared with the oscillation signals as shown in Fig. 2(b). This suggests that a small number of electron-hole pairs were generated by the MIR pulse excitation because the MIR

photon energy (0.26 eV) is much smaller than the band-gap energy (2 eV).

To confirm the properties of the coherent phonons, we performed a fitting of temporal profiles by using the following equation:

$$I(T) = \sum_{i=A_1', E'} A_i \exp(-T/\tau_i) \cos(2\pi f_i T + \phi_i). \quad (1)$$

Here, A_i, τ_i, f_i, and ϕ_i are, respectively, the amplitude, decay time, frequency, and initial phase of the ith mode (E' or A_1'). Figures 3(a)–3(f) show the MIR intensity dependence of the coherent phonon properties (decay time, phase, and frequency) of the E' and A_1' modes. The properties are independent of MIR intensity for both modes, and the frequencies are almost the same as those in Raman spectroscopy [21]. This clearly indicates that anharmonicity of phonons was negligible under the experimental conditions, and the phonon dynamics can be well described by a simple damped harmonic oscillator model, given by

$$\frac{d^2}{dt^2}Q_i + \frac{2}{\tau_i}\frac{d}{dt}Q_i + (2\pi \tilde{f}_i)^2 Q_i = F_i(t), \quad (2)$$

where Q_i and $F_i(t)$ are the normal coordinate and the driving force for the ith mode phonon, respectively, and $\tilde{f}_i$ is given by $[f_i^2 - 1/(2\pi \tau_i)^2]^{1/2}$. Since the pulse width of MIR electric field $\Delta\tau$ (60 fs in full width at half maxima) is shorter than the period of phonon oscillation $1/f_i(>250$ fs) and photon energy (0.26 eV) is far below the band-gap energy ($\sim$2.0 eV), driving force can be regarded as an impulsive force [$F_i(t) = F_i\delta(t)$], and the amplitude of phonon is proportional to F_i. This assumption is justified by the fact that the oscillation phase of phonon motions is independent of MIR intensity as shown in Figs. 3(c) and 3(d), simultaneously indicating that the amount of real carrier generation is negligible in our experiment.
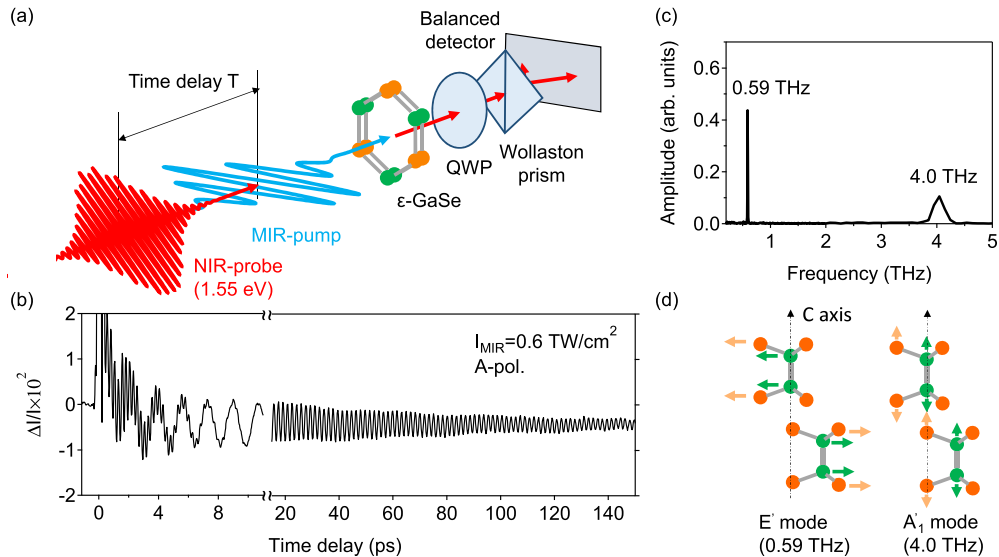
FIG. 2. Coherent phonon spectroscopy in GaSe. (a) Experimental setup of coherent phonon detection in transmission geometry. The angle between the MIR and NIR polarizations was 45°. The polarization modulation of the transmitted NIR probe pulse was detected [20]. (b) Pump-probe signal as a function of time delay with A-pol and MIR intensity of 0.6 TW/cm². Two temporal regions from −1 to 10 ps and from 15 to 150 ps are plotted for clarity. (c) Fourier spectra of the pump-probe signal shown in (b). (d) Schematics of E' and A_1' phonon modes in ε-GaSe. Orange (green) arrows indicate the direction of displacement of the Se (Ga) atom.
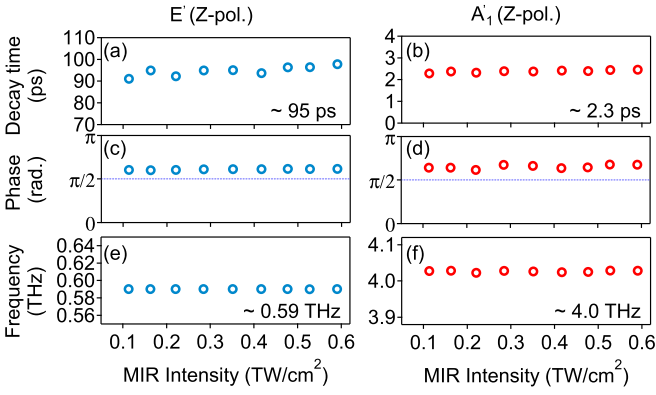
FIG. 3. MIR intensity dependence of coherent phonon properties. Fitting results for E' (A_1') mode with Z-pol are shown in (a), (c), and (e) [(b), (d), and (f)]. Decay time (a), (b), phase (c), (d), and frequency (e), (f) of oscillations are plotted as a function of MIR intensity.

In contrast to its simple dynamics, regarding the amplitude of the phonons, both modes show saturation behavior above 0.3 TW/cm^2 [Figs. 4(a) and 4(b)]. The threshold intensity of saturation depends on the phonon mode and MIR polarization. In the E' mode, much stronger saturation was observed when the MIR polarization was Z-pol than when it was A-pol [Fig. 4(a)]. On the other hand, in the A_1' mode, the saturation behavior was almost independent of the MIR polarization [Fig. 4(b)].

The saturation of phonon amplitude has been already observed in association with the change of frequency and decay time of phonon oscillation under high-density carrier excitation regime, which origin has been attributed to the anharmonic phonon dynamics [22]. On the other hand, we observed saturation without any signature of anharmonic phonon motion and high-density carrier generation as mentioned above. This result suggests that the saturation of phonon amplitude is not due to the phonon anharmonicity, but due to saturation of driving force for phonon F_i in our experiment.

Saturation of the driving force depending on the phonon mode and MIR polarization also cannot be explained by the conventional ISRS process [5,6], where the driving force is proportional to the MIR intensity and its amplitude is independent of the MIR polarization [23]. The fact that saturation threshold intensities are almost the same as those in HHG implies that saturation of the phonon amplitude is also attributed to the nonperturbative light-electron interaction.

To understand the saturation mechanism of the driving force, we can use a simple two-level model with the Born-Oppenheimer approximation to calculate the impulsive force for phonons in the nonperturbative regime. A two-level system linearly coupled with a phonon mode interacting with a light field can be described by the Hamiltonian in the nonperturbative regime, as follows:

$$\hat{H}(t) = \varepsilon_g(Q_i)|g\rangle\langle g| + \varepsilon_e(Q_i)|e\rangle\langle e| + dE_{\mathrm{MIR}}(t)|g\rangle\langle e| + d^*E_{\mathrm{MIR}}(t)|e\rangle\langle g| \tag{3}$$

Here, $|g\rangle$ ($|e\rangle$) is the electronic ground (excited) state with energy of $\varepsilon_g(Q_i)$ [$\varepsilon_e(Q_i)$] with respect to a normal coordinate
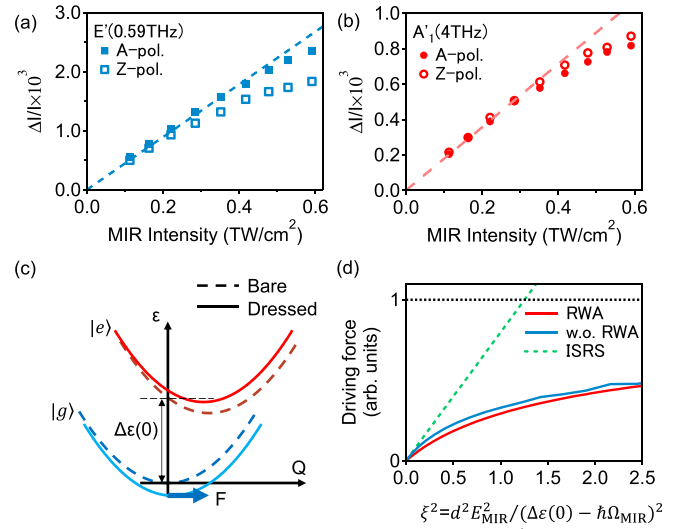
FIG. 4. Saturation of phonon amplitude in extremely nonlinear regime. Amplitude of (a)E' and (b) A_1' phonon modes as a function of MIR intensity. Solid and open squares (circles), respectively, indicate results with A-pol and Z-pol. The dashed lines are guides for the eye that are proportional to MIR intensity. (c) Bare (dashed line) and dressed (solid line) two-level system (g: ground state, e: excited state) depending on phonon coordinate Q in the Frank-Condon picture. Modification of the ground-state energy surface through photon dressing causes a driving force on the phonon. (d) Calculated results of driving force on phonon. Red and blue solid lines, respectively, show the analytical result with the RWA [Eq. (5)] and the numerical result without the RWA. Green dashed line shows the driving force described by the ISRS process. The dotted line indicates the upper limit of the driving force within RWA.

Q_i, which works as an adiabatic potential for the ith mode phonon, as shown by the dashed lines in Fig. 4(c). $d = \langle g|\hat{d}|e\rangle$ is the transition dipole moment between the ground and excited states, and $E_{\mathrm{MIR}}(t)$ is the temporal profile of the MIR electric field.

Without the laser field [$E_{\mathrm{MIR}}(t) = 0$], we assume that the system is in the ground state $|g\rangle$ with no phonon oscillation. Therefore, the driving force of the phonon mode results in

$$F_i = -\left.\frac{\partial \varepsilon_g(Q_i)}{\partial Q_i}\right|_{Q_i=0} = 0 \tag{4}$$

Under an intense laser field, it is hard to neglect the excited state which is mixed coherently with the ground state through the light-electron interaction. One way to solve this problem is the Floquet picture [24,25]. Here, we consider a "dressed" ground (excited) state $|g*\rangle$($|e*\rangle$), whose adiabatic potentials are modified depending on the field strength and frequency of the MIR pulse, as shown in Fig. 4(c). Mixing in the adiabatic potential of the bare excited state $|e\rangle$ gives rise to a finite impulsive driving force in the dressed ground state $|g*\rangle$.

To estimate the impulsive force in the dressed ground state, we first assume continuous nonresonant excitation light $E_{\mathrm{MIR}}(t) = E_{\mathrm{MIR}} \cos(\Omega_{\mathrm{MIR}}t)$ [$\Delta\varepsilon(0) = \varepsilon_e(0) - \varepsilon_g(0) \gg \hbar\Omega_{\mathrm{MIR}}$] and apply the rotating-wave approximation (RWA). With this approximation, we can analytically derive the energy shifts of the driven two-level system in the

nonperturbative regime, i.e., Rabi splitting (optical Stark shift) [26,27], and the driving force as follows [28]:

$$F_i = -\frac{\partial \varepsilon_{g*}(Q_i)}{\partial Q_i}\bigg|_{Q_i=0}$$

$$= -\frac{1}{2}\frac{\partial \varepsilon_e(Q_i)}{\partial Q_i}\bigg|_{Q_i=0}\left(1 - \frac{1}{\sqrt{\xi^2+1}}\right), \qquad (5)$$

$$\xi = \frac{dE_{\text{MIR}}}{\varepsilon_e(0) - \varepsilon_g(0) - \hbar\Omega_{\text{MIR}}}. \qquad (6)$$

Here, ε_{g*} is the (quasi)energy of the dressed ground state, and ξ is the parameter in nonlinear optics for the perturbation expansion [29].

In general, when ξ becomes comparable to unity, a nonperturbative nonlinear optical response such as HHG can be observed. Figure 4(d) plots the driving force of phonon F_i as a function of ξ^2. When ξ is much smaller than 1, F_i is proportional to ξ^2 or $(E_{\text{MIR}})^2$, which is similar to the prediction in the ISRS process (dashed line). On the other hand, when ξ becomes unity, it starts to saturate. Since $\xi \sim 1$ corresponds to $I_{\text{MIR}} \sim 0.3$ TW/cm^2 for our experimental conditions, the calculation is in good agreement with our experimental results showing saturation of the driving force in association with HHG [30].

Moreover, when ξ is much larger than 1, the driving force gradually approaches the upper limit given by half the driving force in the bare excited state $F_i = -[\partial \varepsilon_e(Q_i)/\partial Q_i]/2$. In the strong-field limit, the ratio of the ground to excited states in the dressed ground state becomes unity. Therefore, the driving force for phonon in the dressed state is described as the average of the driving forces in the bare ground and excited states.

To evaluate the driving force more exactly, we performed a numerical calculation without the RWA [33], considering the Bloch-Siegert shift contribution [27,34], which is neglected in Eq. (5). The result is shown by the blue solid line in Fig. 4(d), indicating that the Bloch-Siegert shift contribution introduces a slight increase of the driving force but gives qualitatively the same result as the calculation with the RWA [Eq. (5).] the limit $\xi \ll 1$, the numerical result completely coincides with the theoretical value of the ISRS process. These results provide us an answer to the initial question that there should be a limitation to the nonresonant coherent phonon generation.

In the simple two-level model mentioned above, we neglect anisotropic response as shown in Figs. 4(a) and 4(b), which cannot be explained by ISRS process. This anisotropy is originated from the energy shift of dressed ground state depending on MIR polarization and crystal momentum. By considering a two-band model, which is a natural extension of the two-level model, and the crystal symmetry (D_{3h}), we found that anisotropic response is allowed when highly nonlinear optical process, which is taken into account as Rabi splitting in our model, involves coherent phonon generation process [35]. The observed anisotropy both in HHG yield [Fig. 1(b)] and phonon amplitude saturation [Fig. 4(a)] also supports the validity of our model and suggests the connection between HHG and coherent phonon generation process in nonperturbative regime. We suppose that anisotropic saturation of phonon amplitude reflects an electron-phonon coupling depending on electronic bands and crystal momentum which cannot be accessed by conventional Raman spectroscopy.

In conclusion, we observed coherent phonon generation in the extreme nonlinear regime where nonperturbative nonlinear optical responses such as HHG are observed. Although the phonon dynamics can be described in terms of a damped harmonic oscillator, the phonon amplitude showed saturation depending on the crystal orientation and mode. This saturation behavior can be qualitatively explained by a two-level model with the Born-Oppenheimer approximation and suggests that there is an upper limit to the driving force for the phonon mode in the nonresonant laser excitation. This scenario applies not only to phonons but also to other quasiparticles, such as magnons [36], and suggests that we need precise control of driving electric field or alternative means such as direct excitation of quasiparticles in order to realize the formation of macroscopic ordering through the large-amplitude driving of quasiparticles.

[1] D. Fausti, R. I. Tobey, N. Dean, S. Kaiser, A. Dienst, M. C. Hoffmann, S. Pyon, T. Takayama, H. Takagi, and A. Cavalleri, Science **331**, 189 (2011).

[2] E. J. Sie, C. M. Nyby, C. D. Pemmaraju, S. J. Park, X. Shen, J. Yang, M. C. Hoffmann, B. K. Ofori-Okai, R. Li, and A. H. Reid *et al.*, Nature (London) **565**, 61 (2019).

[3] A. Von Hoegen, R. Mankowsky, M. Fechner, M. Först, and A. Cavalleri, Nature (London) **555**, 79 (2018).

[4] M. Först, C. Manzoni, S. Kaiser, Y. Tomioka, Y. Tokura, R. Merlin, and A. Cavalleri, Nat. Phys. **7**, 854 (2011).

[5] Y. X. Yan, E. B. Gamble, and K. A. Nelson, J. Chem. Phys. **83**, 5391 (1985).

[6] R. Merlin, Solid State Commun. **102**, 207 (1997).

[7] M. Wegener, *Extreme Nonlinear Optics* (Springer-Verlag, Berlin, 2005).

[8] S. Ghimire, A. D. DiChiara, E. Sistrunk, P. Agostini, L. F. DiMauro, and D. A. Reis, Nat. Phys. **7**, 138 (2011).

[9] A. Schiffrin, T. Paasch-Colberg, N. Karpowicz, V. Apalkov, D. Gerster, S. Mühlbrandt, M. Korbman, J. Reichert, M. Schultze, and S. Holzner *et al.*, Nature (London) **493**, 70 (2013).

[10] H. Liu, Y. Li, Y. S. You, S. Ghimire, T. F. Heinz, and D. A. Reis, Nat. Phys. **13**, 262 (2017).

[11] Y. S. You, D. A. Reis, and S. Ghimire, Nat. Phys. **13**, 345 (2016).

[12] S. Ghimire and D. A. Reis, Nat. Phys. **15**, 10 (2019).

[13] O. Schubert, M. Hohenleutner, F. Langer, B. Urbanek, C. Lange, U. Huttner, D. Golde, T. Meier, M. Kira, S. W. Koch, and R. Huber, Nat. Photonics **8**, 119 (2014).

[14] M. Hohenleutner, F. Langer, O. Schubert, M. Knorr, U. Huttner, S. W. Koch, M. Kira, and R. Huber, Nature (London) **523**, 572 (2015).

[15] F. Langer, M. Hohenleutner, U. Huttner, S. W. Koch, M. Kira, and R. Huber, Nat. Photonics **11**, 227 (2017).

[16] S. Jandl, J. L. Brebner, and B. M. Powell, Phys. Rev. B **13**, 686 (1976).

[17] W. A. Kütt, W. Albrecht, and H. Kurz, IEEE J. Quantum Electron. **28**, 2434 (1992).

[18] See Supplemental Material at http://link.aps.org/supplemental/10.1103/PhysRevB.101.094301 for the description of the Z-scan measurements using the same MIR pump in GaSe (see also Ref. [19] therein, which gives information about dielectric function of GaSe) in Sec. 2.

[19] C.-W. Chen, T.-T. Tang, S.-H. Lin, J. Y. Huang, C-S. Chang, P.-K. Chung, S.-T. Yen, and C.-L. Pan, J. Opt. Soc. Am. B **26**, A58 (2009).

[20] See Supplemental Material at http://link.aps.org/supplemental/10.1103/PhysRevB.101.094301 for the description of the probing scheme of coherent phonon in Sec. 3.

[21] R. M. Hoff, J. C. Irwin, and R. M. A. Lieth, Can. J. Phys. **53**, 1606 (1975).

[22] O. V. Misochko, M. Hase, K. Ishioka, and M. Kitajima, Phys. Rev. Lett. **92**, 197401 (2004).

[23] See Supplemental Material at http://link.aps.org/supplemental/10.1103/PhysRevB.101.094301 for the description of the polarization selection rule of ISRS in GaSe in Secs. 3 and 7.

[24] J. H. Shirley, Phys. Rev. **138**, B979 (1965).

[25] Y. Shinohara, K. Yabana, Y. Kawashita, J.-I. Iwata, T. Otobe, and G. F. Bertsch, Phys. Rev. B **82**, 155110 (2010).

[26] J. S. Bakos, Phys. Rep. **31**, 209 (1977).

[27] E. J. Sie, C. H. Lui, Y.-H. Lee, L. Fu, J. Kong, and N. Gedik, Science **355**, 1066 (2017).

[28] See Supplemental Material at http://link.aps.org/supplemental/10.1103/PhysRevB.101.094301 for the description of the derivation of driving force for phonon in Sec. 4.

[29] R. W. Boyd, *Nonlinear Optics* (Academic, New York, 2008).

[30] See Supplemental Material at http://link.aps.org/supplemental/10.1103/PhysRevB.101.094301 for the description of the fitting results (see also Refs. [31,32] therein, which gives information about the oscillator strength of interband transition) in Sec. 4.

[31] A. F. Qasrawi, Cryst. Res. Technol. **40**, 610 (2005).

[32] A. F. Qasrawi and A. A. Saleh, Cryst. Res. Technol. **43**, 769 (2008).

[33] See Supplemental Material at http://link.aps.org/supplemental/10.1103/PhysRevB.101.094301 for the description of the driving force for phonon without RWA in Sec. 5.

[34] F. Bloch and A. Siegert, Phys. Rev. **57**, 522 (1940).

[35] See Supplemental Material at http://link.aps.org/supplemental/10.1103/PhysRevB.101.094301 for the description of the anisotropy of driving force for phonon in Secs. 6 and 7.

[36] A. Kirilyuk, A. V. Kimel, and T. Rasing, Rev. Mod. Phys. **82**, 2731 (2010).